

Path tracking control of self-reconfigurable robot hTetro with four differential drive units

Yuyao Shi¹, Mohan Rajesh Elara², Anh Vu Le³, Veerajagadheswar Prabakaran⁴ and Kristin L. Wood⁵

Abstract—The research interest in mobile robots with independent steering wheels has been increasing over recent years due to their high mobility and better payload capacity over the systems using omnidirectional wheels. However, with more controllable degrees of freedom, almost all of the platforms include redundancy, which are modeled using the instantaneous center of rotation (ICR). This paper deals with a Tetris-inspired floor cleaning robot hTetro which consists of four interconnected differential-drive units. Each module has a differential drive unit which can steer individually. Differing from most other steerable wheeled mobile robots, the wheel arrangement of this robot changes because of its self-reconfigurability. In this paper, we proposed a path tracking controller that can handle discontinuous trajectories and sudden orientation changes for hTetro. Singularity problems are resolved on both the mechanical aspect and the control aspect. The controller is tested experimentally with the self-reconfigurable robotic platform hTetro, and results are discussed.

I. INTRODUCTION

The concept of modular and self-reconfigurable mechanisms are widely used due to its robustness, adaptability and multi-functionality. Self-reconfigurable robots are usually composed of multiple modules and able to perform shape-shifting according to different circumstances. A variety of reconfigurable systems have been developed to complete a wide range of tasks [1][2]. The system addressed in this paper is a self-reconfigurable robot developed for the floor-cleaning purpose. Inspired from the Tetris game, hTetro was designed to have four modular blocks, which allow hTetro to transform into seven configurations as shown in Fig. 1c. This enables it to access narrow spaces and increases the area coverage as proved in [3][4]. The advantages of using linked modular-type robot over multiple independent units are 1) the former is not limited by means of data transfer as the signals are transmitted through wires. 2) The requirement of computational power is lower for controlling one unit comparing to multiple units. Thus, with the same ability in area coverage,

the self-reconfigurable robotic architecture has lesser requirements for the sensors, communication modules, actuators and other hardware. The platform introduced in this paper is a robust version of hTetro which uses four differential drive modules and free hinges instead of mecanum wheels with actuated servo hinges [3]. By using a differential drive against four mecanum wheels in each module [3], hTetro is capable of moving on uneven terrain such as carpet or cemented granular. In [3][4], active hinge joints were used to change the configuration, which results in using of additional servos for reconfiguration and leads to low robustness due to servo break down. The modified design presented here uses free hinged joints with suspension. Electromagnets are used to maintain the specific configuration during locomotion while transformation is done by decoupling electromagnets and driving the modules individually. The independent steering action in each of the four modules gained using differential wheel action. [4].

The difficulty in controlling a robot with multiple steering modules lies upon satisfying the rigid body kinematic constraints. Lee and Tzoo-Hseng proposed a kinematic and dynamic control law based on the Lyapunov method and verified the stability in simulation [5]. The drawback with this method is that it does not consider the non-holonomic constraints of the platform during the modeling which in practice will lead to improper alignment of wheels and cause tire wear because of the skidding motion. Some of the solutions are to design mechanical linkages between the wheels to prevent conflict in steering angles [6][18][8]. However, the additional mechanical linkage limits the steering angle and results in lesser maneuverability. It is also not suitable in this reconfigurable platform.

Modeling the platform under the instantaneous center of rotation (ICR) space is an alternative method.

Although using the ICR and individual steering wheel configuration ensures the stability, there are singularity problems associated with it. The singularity happens on two aspects, namely, representation aspect and numerical aspect. The former refers to the situation where the steerable wheels are parallel with each other. In this case, the ICR is theoretically located at infinity. In order to solve the representational singularity, coordinate switching is one of the proposed methods [9][10]. The latter refers to the situation where the ICR is located along the steering axes. In this case, there are more than one solutions to the desired angular velocity. This singularity has been addressed using artificial potential fields, as reported in [9][11][12][?] or by offsetting the steering axis outside of the wheel plane [13][14][15]. However, the usage

*This work is supported by Singapore National Robotics R&D Program Office and SUTD-MIT International Design Center.

¹Y. Shi is with the Department of Engineering Product Development (EPD), Singapore University of Technology and Design (SUTD), Singapore, 487372, yuyao_shi@sutd.edu.sg

²M. R. Elara is with Department of EPD, SUTD, Singapore, 487372, rajesh_mohan@sutd.edu.sg

³A. V. Le is with Optoelectronics Research Group, Faculty of Electrical and Electronics Engineering, Ton Duc Thang University, Ho Chi Minh City 700000, Vietnam, leanhvu@tdtu.edu.vn

⁴V. Prabakaran is with Department of EPD, SUTD, Singapore, 487372, prabakaran@sutd.edu.sg

⁵K. L. Wood is the associate provost (graduate studies), Co-director of SUTD-MIT International Design Centre, SUTD, Singapore, 487372, kristinwood@sutd.edu.sg

of artificial potential field limited the position of ICR while offsetting the steering axis leads to the coupling between steering and propulsion motion [7]. In all the method proposed, the control problem is complicated either because of considering the coupling between steering and propulsion motion or involving dynamic control [16][17][18]. However, in this approach, the usage of differential drive solved the numerical singularity while not coupling the steering and propulsion motion. Therefore, the controller proposed in this paper is only based on kinematics of the robot which is simpler than dynamic control.

The earlier version of hTetro also made use of the in-differential steering drive mechanism [20]. Predefined-Radius-Lo-motion (PRL) and Fixed-Heading-Angle-Lo-motion (FHAL) were performed to test the maneuverability of the robot. The transformation mechanism of hTetro was also illustrated in detail. However, no path tracking control strategy and singularity avoidance were considered.

The main contributions of this paper focus on two aspects. Firstly, a mechanical design that avoids the singularity where ICR is located at the steering center. By using differential drive, the numerical singularity problem can be avoided naturally without complicating the kinematics. Secondly, a path tracking controller that fits different wheel arrangements. The controller can be considered as two layers: a higher level controller to determine the ICR and the corresponding steering angles, and a lower level controller on the module level to ensure the kinematic constraints during transient state.

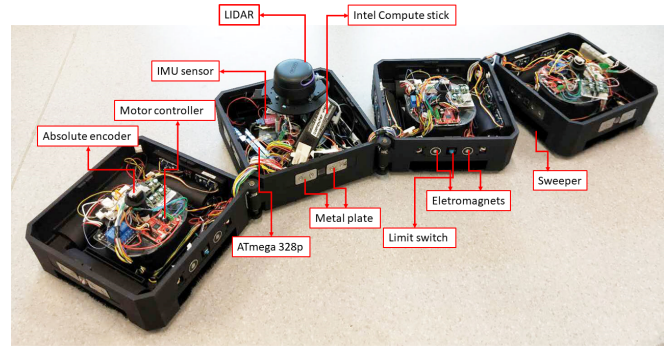
The paper is organized into five sections. The mechanical design of hTetro and its kinematic model based on instantaneous center of rotation is presented in Section II. Section III describes the controller design and the method to avoid conflicting the kinematic constraints. The robust mechanical design and control is supported by experiments in Section IV. Section V concludes with future works.

II. KINEMATIC MODEL

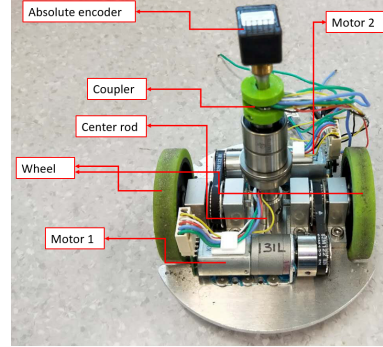
In this section, the mechanical design and the system architecture of the current hTetro platform are presented. A kinematic formulation is also developed in Section II-B which is different from that of the normal fixed morphology robot because of its reconfigurability.

A. Robot description and modeling parameters

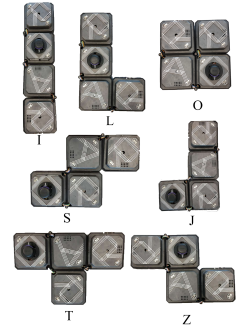
The platform, as shown in Fig. 1a, consists of four modules connected by three free hinges with suspensions. Each module has a differential-drive locomotion module driven by two 12V DC motors. The locomotion modules are connected with the four chassis through the bushing on the central rod. Hence, the heading angles of the locomotion modules are independent of the orientations of their corresponding chassis as well as that of the whole robot. With respect to electronics, we separated it as global and local peripheries. The global components such as LIDAR, IMU, and compute stick act as a top layer which helps the robot to perform simultaneous localization and mapping



(a) Hardware design of the current hTetro



(b) Hardware design of the locomotion module



(c) 7 configurations of hTetro

Fig. 1: Mechanical design and hardware placement

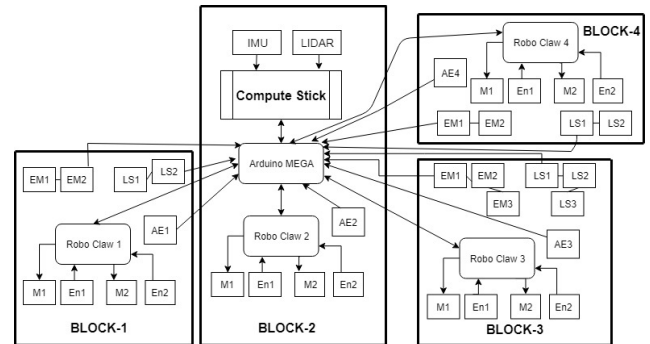


Fig. 2: hTetro System Architecture

(SLAM), and autonomous navigation. Since block 2 acts as an anchor point for hTetro, we align the orientation of the whole robot with that of the second block. The local components such as motor driver (Roboclaw), electromagnet (EM), limit switch (LS), absolute encoders (AE) motors (M), and its encoders (En) would execute the reconfiguration and locomotion of hTetro. Electromagnets were used to maintain the morphology during navigation. Limit switches were used to ensure the completion of reconfiguration and to detect the morphology failures. Except in block 2, we housed two sets of electromagnets and limit switches in block 1, and block 4 and three sets in block 3. For locomotion, we have a set of motor driver, motor, and encoders in each block. We used Roboclaw motor driver to control the motors and to collect the encoder signals which would be transferred to the local

TABLE I: modeling Parameters

Symbols	Description
\mathcal{F}_I	World frame
\mathcal{F}_b	Robot frame
X^*, Y^*	Current position of COG w.r.t. frame \mathcal{F}_I
X_d^*, Y_d^*	Desire position of COG w.r.t. frame \mathcal{F}_I
θ^*	Current orientation of the robot w.r.t. frame \mathcal{F}_I
θ_d^*	Desire orientation of the robot w.r.t. frame \mathcal{F}_I
θ_e	Orientation error
\mathcal{F}_{bi}	Individual frame at steering axis of i^{th} module
β_i	Steering angle w.r.t. chasis-fixed frame \mathcal{F}_{bi}
α_j	Angle at j^{th} hinge
X_e^*, Y_e^*	Position error under \mathcal{F}_b
R	Current instantaneous radius of rotation under \mathcal{F}_b
γ	Current driving angle of the robot under \mathcal{F}_b
R_d	Desire instantaneous radius of rotation under \mathcal{F}_b
γ_d	Desire driving angle of the robot under \mathcal{F}_b
ϕ_{iL}, ϕ_{iR}	rotational speed of i^{th} module's left/right wheel
v_i	Linear speed of i^{th} module
r_w	Wheel radius
d	Wheel to center distance
l	Length of each module

controller. On top of every locomotion module, we housed an absolute encoder (AE) that could sense the heading angle of each locomotion module and send the data back to the controller. Almost every local peripheral's data acquisition is done by the local controller for which we employed Arduino MEGA that is housed in block 2. Arduino Mega is the only local component that communicates with compute stick and distributes commands to low-level peripherals to perform the tasks effectively. The detailed system architecture of hTetro is shown in Fig. 2. The assumptions made during the modeling are 1) The robot does not perform shape changing during locomotion. In other words, it is treated as a rigid platform during the locomotion, 2) The wheels roll with no slipping and no skidding during the locomotion. The legends for the symbols used are described in TABLE I (see also Fig. 3).

B. Kinematic modeling

Fig. 3 shows a schematic plot of the mobile robot w.r.t. the world inertial frame \mathcal{F}_I . The position of the robot is defined as the position of the centroid from the top view and the orientation is defined by the orientation of LIDAR which imposes the orientation of the chassis of the second module. Each individual module is separated from the others. So for each differential drive module, it has $v_i = \frac{1}{2}r_w(\phi_{iL} - \phi_{iR})$ and $\dot{\beta}_i = \frac{1}{2}r_w(\phi_{iL} + \phi_{iR})$. Let $\xi^* = [x^* \ y^* \ \theta^*]^T$ be the 3D task space coordinate under \mathcal{F}_I and ξ_d^* denotes the desire one. The position of the centroid of the platform O_b is defined to be $[\frac{\sum_{i=1}^4 x_i}{4}, \frac{\sum_{i=1}^4 y_i}{4}]$ where x_i and y_i are the position of the steering axis of each block i w.r.t. the inertial frame (\mathcal{F}_I). By treating each locomotion module as a whole, the forward kinematics of the robot can be expressed as:

$$\dot{\xi}^* = \mathbf{R}(\theta)\mathbf{G}\mathbf{v} \quad (1)$$

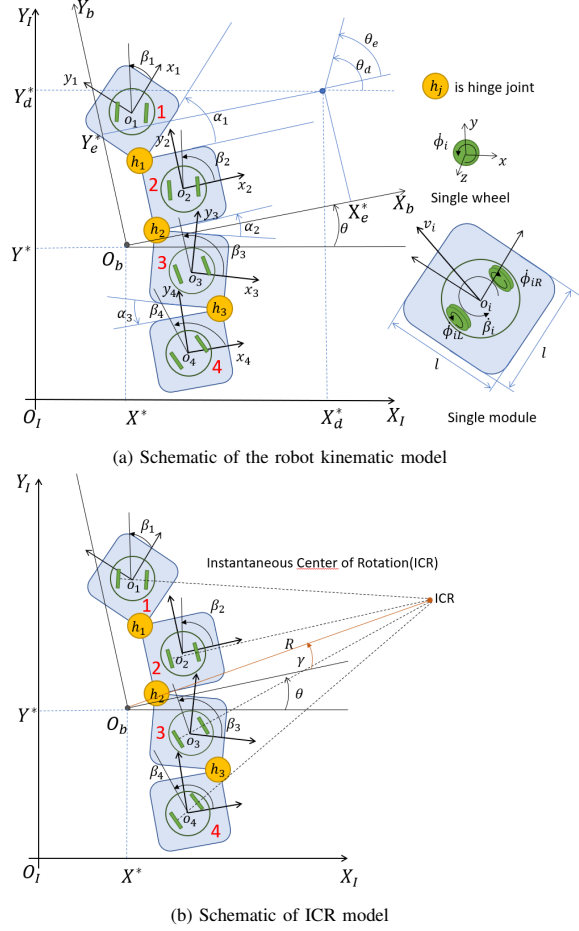


Fig. 3: Schematic diagrams of hTetro.

with $\mathbf{v} = [v_1 \ v_2 \ v_3 \ v_4]^T$ and $\mathbf{G}^T =$

$$\begin{bmatrix} \cos(\beta_1 + \alpha_1) & \sin(\beta_1 + \alpha_1) & \frac{\overline{O_b O_1}^\perp}{4|\overline{O_b O_1}|^2} \\ \cos(\beta_2) & \sin(\beta_2) & \frac{\overline{O_b O_2}^\perp}{4|\overline{O_b O_2}|^2} \\ \cos(\beta_3 + \alpha_2) & \sin(\beta_3 + \alpha_2) & \frac{\overline{O_b O_3}^\perp}{4|\overline{O_b O_3}|^2} \\ \cos(\beta_4 + \alpha_2 + \alpha_3) & \sin(\beta_4 + \alpha_2 + \alpha_3) & \frac{\overline{O_b O_4}^\perp}{4|\overline{O_b O_4}|^2} \end{bmatrix}$$

The last column of \mathbf{G}^T is to get the orthogonal projection of \mathbf{v} on the line connecting the centroid of the platform and that of each module. $\mathbf{R}(\theta)$ is the transformation matrices from \mathcal{F}_b to \mathcal{F}_I .

In addition, with the assumption that no reconfiguration is allowed during locomotion, θ^* is defined to be the angular velocity at the centroid of the current shape which coincide with the angular velocities of all four chassis. The inverse kinematics is found through pseudo inverse of the forward kinematics.

However, as the platform is a redundant system, only using pseudo inverse to get the inverse kinematics does not ensure that the kinematic constraints are fulfilled. Therefore, the actuation command of each motor is regulated with respect to the ICR placement which will be discussed in the following section.

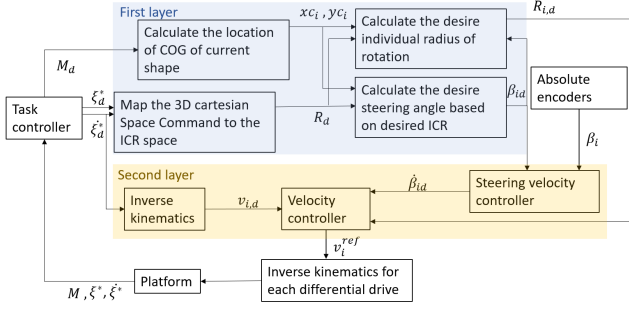


Fig. 4: Control framework of hTetro

III. PATH TRACKING CONTROLLER DESIGN

In this section, the control framework for hTetro are presented, including locating of ICR, steering angles calculation, and controller design. The schematic diagram of the control framework is shown in Fig. 4. In order to perform the cleaning task, the platform navigation is based on waypoints which contain the information of the desired position and orientation. Only when the platform reaches the waypoint correctly, the next waypoint information will be given. In between two waypoints, the centroid of the robot is required to follow a straight path while tracking the desired orientation. During the process above, the desired position and velocity (ξ^* , $\dot{\xi}^*$) were given by a high-level perception controller and then mapped to find the desired location of instantaneous center of rotation (ICR_d). Inspired from the previous work [10], the position of the ICR_d is expressed using polar coordinates assigned with \mathcal{F}_b . The output is then used to calculate the desired corresponding steering angles (β_{id}), and individual radius of rotation (r_i). These information are fed into the individual steering angle controller together with the current instantaneous center of rotation to determine the angular velocity ($\dot{\beta}_{id}$) of each steering module. After that, due to the speed limit of the motor, a velocity controller will be used to regulate the desired linear velocity of each module ($v_{i,d}$) to generate the corresponding angular velocity (ϕ_{iL}^{real} and ϕ_{iR}^{real}) of each wheel.

A. First Layer: Locating Desired Instantaneous Center of Rotation

As shown in Fig. 4, desired position (X_d^*, Y_d^*) on the reference trajectory and current position (X^*, Y^*), the error defined under robot frame is defined by:

$$\begin{bmatrix} X_e^* \\ Y_e^* \end{bmatrix} = \begin{bmatrix} \cos(\theta^*) & -\sin(\theta^*) \\ \sin(\theta^*) & \cos(\theta^*) \end{bmatrix} \begin{bmatrix} X_d^* - X^* \\ Y_d^* - Y^* \end{bmatrix} \quad (2)$$

The position error information is used to generate the angular coordinate of the desired ICR location (γ_d) which is defined to be

$$\gamma_d = \arctan\left(\frac{Y_e^*}{X_e^*}\right) \quad (3)$$

It indicates that when there is only an error in the position, γ_d will be the driving direction of the robot. On the other hand, when there also exists error in the orientation, the desired radius of rotation is estimated by treating the whole platform

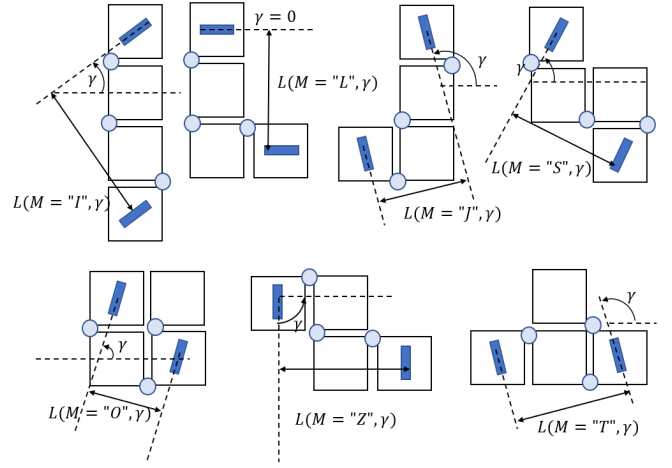


Fig. 5: Definition of $L(M, \gamma)$ under seven different morphology.

as a two wheel differential drive robot. The two wheels with the maximum distance between their x-y planes are modeled to be the two wheels of the differential-drive as shown in Fig. 5. It is because the maximum and the minimum velocity will only occur at these two modules. Thus, taking the two wheels with the maximum distance ensure the desired radius of the curvature does not exceed the hardware limit. Hence, the distance between the two modules is defined to be the width between the two equivalent wheels. Knowing that $\theta_e = \theta_d^* - \theta^*$, the desired angular velocity of the equivalent differential-drive model is controlled by a proportion controller with an adaptive gain $\dot{\theta}_d = k_p \theta_e$.

The equivalent left wheel velocity (v_l') and right wheel velocity (v_r') for the differential-drive model are estimated by

$$\begin{cases} v_r' = \text{sign}(\dot{X}_d^*) \sqrt{Y_d^{*2} + X_d^{*2}} - L(M, \gamma) \dot{\theta}_d \\ v_l' = \text{sign}(\dot{X}_d^*) \sqrt{Y_d^{*2} + X_d^{*2}} + L(M, \gamma) \dot{\theta}_d \end{cases} \quad (4)$$

where $L(M, \gamma)$ refers to the perpendicular distance between the equivalent wheels for the particular morphology M with the current driving angle. Also, $\text{sign}(\dot{X}_d^*)$ is the signum function which gives -1 when $\dot{X}_d^* < 0$ or 1 when $\dot{X}_d^* \geq 0$. It is used to cover the two dimensional ICR space as $\gamma_d \in [-\frac{\pi}{2}, \frac{\pi}{2}]$. Therefore, the instantaneous radius of rotation derived from (4) can be represented as

$$R_d = \frac{L(M, \gamma) v_l' + v_r'}{2 v_l' - v_r'} = \frac{\text{sign}(\dot{X}_d^*) \sqrt{Y_d^{*2} + X_d^{*2}}}{\dot{\theta}_d} \quad (5)$$

However, there exist a singularity point when $\dot{\theta}_d = 0$ in (5). An alternative method to constrain the radius is proposed below using hyperbolic tangent function with a large value R_{max} considering the resolution of the absolute encoders.

$$R_d = R_{max} \tanh\left(\frac{\sqrt{Y_d^{*2} + X_d^{*2}}}{\dot{\theta}_d R_{max}}\right) \quad (6)$$

The location of ICR_d under \mathcal{F}_b is defined by the desired tangential driving angle γ_d and the radius R_d which separates

the linear motion and the angular motion of hTetro. It allows hTetro platform to correct either of the attributes, i.e., position and orientation while maintaining the other.

B. Second Layer: Individual Steering Velocity Controller

The hTetro is able to change to seven different shapes and the relative position of each locomotion module also changes. The position of the steering axes with respect to \mathcal{F}_b are denoted as (x_i^c, y_i^c) with $i \in \{1, 2, 3, 4\}$. After that, the desired steering angle $(\beta_{i,d})$ and individual instantaneous radius of rotation (r_i) of each module are given by:

$$\beta_{i,d} = \arctan\left(\frac{y_i^c - R_d \sin(\gamma_d)}{R_d \cos(\gamma_d) - x_i^c}\right) - \alpha_j \quad (7)$$

$$r_i = \frac{y_i^c - R_d \sin(\gamma_d)}{\sin(\beta_{i,d})} \quad (8)$$

$$\text{while } \alpha_j = \begin{cases} \alpha_1 & i = 1 \\ 0 & i = 2 \\ \alpha_2 & i = 3 \\ \alpha_2 + \alpha_3 & i = 4 \end{cases}$$

Because the control signals $(\dot{\beta}_{i,d})$ are error driven, when discontinuous signal is given, for instance, when the robot arrived at the waypoint, it is likely that the required motor speed exceeds its hardware limit. Hence, a constrained feedback controller is used to regulate the linear velocities (v_i) which is illustrated in Section III-C. From the absolute encoder, as shown in Fig. 1b, the current steering angle of each locomotion module (β_i) is used to compare the difference. The initial steering angles are determined according to the ICR_d at that instant. The desired steering velocities are controlled according to the steering error $\beta_{i,e} = \beta_{i,d} - \beta_i$ such that the kinematic constraint are fulfilled during the transition period. In other words, the controller is used to ensure the lines, which are perpendicular to each wheel plane and passes through the centroid of each module, as expressed in (9) are always concurrent when $v_i \neq 0$ because the four locomotion modules are indifferent when $v_i = 0$. The α_j used in (9) are defined the same way as (7).

$$-\frac{1}{\tan(\beta_i + \alpha_j)}(x - x_i^c) = (y - y_i^c) \quad (9)$$

(9) can be written in the form $\mathbf{A}\mathbf{x} = \mathbf{b}$ where $\mathbf{x} = [x \ y]^T$ and \mathbf{A} is the coefficient matrix of the individual radius of rotation. Then, its augmented matrix

$$[\mathbf{A}|\mathbf{b}] = \left[\begin{array}{cc|cc} \frac{-1}{\tan(\beta_1 + \alpha_1)} & -1 & \frac{-1}{\tan(\beta_1 + \alpha_1)}x_1^c + y_1^c & \\ \frac{-1}{\tan(\beta_2)} & -1 & \frac{-1}{\tan(\beta_2)}x_2^c + y_2^c & \\ \frac{-1}{\tan(\beta_3 + \alpha_2)} & -1 & \frac{-1}{\tan(\beta_3 + \alpha_2)}x_3^c + y_3^c & \\ \frac{-1}{\tan(\beta_4 + \alpha_2 + \alpha_3)} & -1 & \frac{-1}{\tan(\beta_4 + \alpha_2 + \alpha_3)}x_4^c + y_4^c & \end{array} \right] \quad (10)$$

With the initialization of the steering angles, it is known that $\text{rank}(\mathbf{A}_{init}|\mathbf{b}_{init}) = \text{rank}(\mathbf{A}_{init}) \leq 2$ which means all four lines that are co-linear with radii are either parallel or concurrent. Similarly, we also know that at the final state all the steering angles should fulfill the kinematic constraint which indicates that $\text{rank}(\mathbf{A}_d|\mathbf{b}_d) = \text{rank}(\mathbf{A}_d) \leq 2$. Hence,

TABLE II: Relationships among x_i^c or y_i^c

shape	x_i^c relationship	y_i^c relationship
I	$x_1^c = x_2^c = x_3^c = x_4^c = 0$	$y_1^c = 3y_2^c = -3y_3^c = -y_4^c$
L	$x_1^c = x_2^c = x_3^c = -x_4^c$	$y_1^c = 3y_2^c = -3y_3^c = y_4^c$
Z	$x_1^c = x_4^c, x_2^c = x_3^c = 0$	$y_1^c = y_2^c = -y_3^c = -y_4^c$
O	$x_1^c = x_2^c = -x_3^c = -x_4^c$	$y_1^c = -y_2^c = -y_3^c = y_4^c$
T	$x_1^c = -3x_2^c = x_3^c = x_4^c$	$y_1^c = -y_4^c, y_2^c = y_3^c = 0$
S	$x_1^c = x_3^c = 0, x_2^c = -x_4^c$	$y_1^c = y_2^c = -y_3^c = -y_4^c$
J	$-x_1^c = x_2^c = x_3^c = x_4^c$	$y_1^c = y_2^c = -3y_3^c = -y_4^c$

these two situations will be illustrated separately in Section III-B.1 and Section III-B.2.

1) Both initial state and desired state are parallel:

Under this situation, $\dot{\theta}_d = 0$ and $\beta_{i,e} = \gamma_d - \gamma$ which means the robot only perform translational motion. The ranks of the coefficient and augmented matrices are one. Therefore, the steering velocity profiles of all four modules should be the same. In this case, a PID controller was used to keep the heading angle unchanged. Therefore, $\dot{\beta}_i(t) = k_p \gamma_e(t) + k_i \int_0^t \gamma_e(t) dt + k_d \frac{d\gamma_e(t)}{dt}$. As the initial state with an arbitrary γ could satisfy the constraint, substituting β_i with $\beta_i + \int_0^t \dot{\beta}_i(t) dt$ will not violate the constraint as well.

2) Either initial state or desired state is concurrent:

When the initial or final state is concurrent, the solution for the system is unique, indicating ranks of both matrices are two. By doing row-echelon reduction and rearranging the column of the the augmented matrix, matrix \mathbf{A} and vector \mathbf{b} can be express as (11).

$$\mathbf{A} = \begin{bmatrix} 1 & \frac{1}{\tan(\beta_1 + \alpha_1)} \\ 0 & \frac{1}{\tan(\beta_2)} - \frac{1}{\tan(\beta_1 + \alpha_1)} \\ 0 & \frac{1}{\tan(\beta_3 + \alpha_2)} - \frac{1}{\tan(\beta_1 + \alpha_1)} \\ 0 & \frac{1}{\tan(\beta_4 + \alpha_2 + \alpha_3)} - \frac{1}{\tan(\beta_1 + \alpha_1)} \end{bmatrix} \quad (11)$$

$$\mathbf{b} = \begin{bmatrix} \frac{1}{\tan(\beta_1 + \alpha_1)}x_1^c + y_1^c \\ \frac{1}{\tan(\beta_2)}x_2^c - \frac{1}{\tan(\beta_1 + \alpha_1)}x_1^c + y_2^c - y_1^c \\ \frac{1}{\tan(\beta_3 + \alpha_2)}x_3^c - \frac{1}{\tan(\beta_1 + \alpha_1)}x_1^c + y_3^c - y_1^c \\ \frac{1}{\tan(\beta_4 + \alpha_2 + \alpha_3)}x_4^c - \frac{1}{\tan(\beta_1 + \alpha_1)}x_1^c + y_4^c - y_1^c \end{bmatrix} \quad (12)$$

Due to the geometry property of the seven configurations, the relationship among all x_i^c or among y_i^c are summarized in TABLE.II.

As a result, by substituting the relationships in TABLE.II to (11), it can be found that the following relationship between the steering angles should be fulfilled.

$$\frac{1}{\tan(\beta_1 + \alpha_1)} - C_1 \frac{1}{\tan(\beta_2)} - C_2 \frac{1}{\tan(\beta_3 + \alpha_2)} - C_4 \frac{1}{\tan(\beta_4 + \alpha_2 + \alpha_3)} = 0 \quad (13)$$

The relationship above is derived by assuming the system is consistent. C_i are constant coefficient for different shapes with respect to TABLE.II. Due to the assumption made in Section II-B, the relationships among x_i^c and y_i^c will not change during locomotion. Thus, in order to fulfill the

concurrent requirement, $\dot{\beta}_i(t)$ should be restricted by the following constraints as expressed in 14 and 15.

$$\int_0^{t_{final}} \dot{\beta}_i(t) dt = \beta_{i,e} \quad (14)$$

This constraint is to ensure it reaches the desired angle at the same time instance t_{final} .

$$\tan(\beta_{i,init} + \int_0^t \dot{\beta}_i(t) dt + \alpha_j) = \lambda \tan(\beta_{i,init} + \alpha_j) \quad (15)$$

or

$$\tan(\beta_{i,init} + \int_0^t \dot{\beta}_i(t) dt + \alpha_j) = \lambda \tan(\beta_{i,d} + \alpha_j) \quad (16)$$

This is to ensure the kinematic constraint during the transient state depending on the concurrent relationship.

Initially, β_i^+ is defined to be the desired velocity of the first time instance.

$$\beta_i^+ = \int_0^{t^+} \dot{\beta}_i^+ dt \quad (17)$$

Substitute (17) into (15) and $t = t^+$,

$$\beta_{i,e}^+ = \beta_{i,e} - \beta_i^+ \quad (18)$$

$$\tan(\beta_{i,init} + \beta_i^+ + \alpha_j) = \frac{\tan(\beta_{i,init} + \alpha_j) + \tan(\beta_i^+)}{1 - \tan(\beta_{i,init} + \alpha_j) \tan(\beta_i^+)} \quad (19)$$

Hence,

$$\lambda = \frac{1 + \frac{\tan(\beta_i^+)}{\tan(\beta_{i,init} + \alpha_j)}}{1 - \tan(\beta_i^+)} = \frac{1 + \frac{\tan(\beta_i^+)}{\tan(\beta_{i,d} + \alpha_j)}}{1 - \tan(\beta_i^+)} \quad (20)$$

In order to ensure the linear dependency is followed by all four module, λ is defined by substituting the maximum β_i in to (17) which is determined by the maximum $\beta_{i,e}$ to fulfill criteria (14) through a PID controller. Thus, the module with the maximum error will be used as reference to calculate the λ . After that, the rest of the steering angles (β_i^+) are calculated based on (20) which is then used to determine the steering speed of the rest modules ($\dot{\beta}_i$).

C. Constraint Individual Velocity Controller

According to Section III, a constraint velocity controller need to be implemented to restrict the maximum drive rate of each motor. Referring to (8) and (5), the desired linear velocity of each module can be expressed as

$$v_{id} = \frac{r_i}{R_d} \sqrt{Y_d^{*2} + X_d^{*2}} = \frac{r_i}{R_d} \dot{\theta}_d = \frac{r_i}{R_d} k_p (\theta_d - \theta) \quad (21)$$

the desired drive rate of each wheel motor for each module i is given as:

$$\dot{\phi}_{iL} = \frac{\dot{\beta}_i}{r_w} + \frac{v_{id}}{r_w}, \quad \dot{\phi}_{iR} = \frac{\dot{\beta}_i}{r_w} - \frac{v_{id}}{r_w} \quad (22)$$

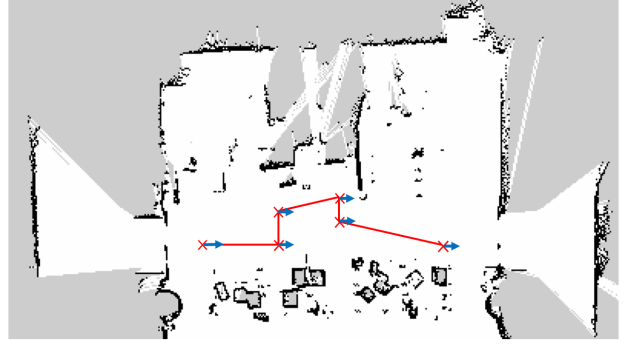


Fig. 6: 2D map used for the experiment

Substituting (21) into (22),

$$\dot{\phi}_{iL} = \frac{\dot{\beta}_i d}{r_w} + \frac{\frac{r_i}{R_d} k_p (\theta_d - \theta)}{r_w} \quad (23)$$

$$\dot{\phi}_{iR} = \frac{\dot{\beta}_i d}{r_w} - \frac{\frac{r_i}{R_d} k_p (\theta_d - \theta)}{r_w} \quad (24)$$

In order for the drive rate not to exceed the drive limit $\dot{\phi}_{max}$ according to the hardware limitation of the motor, k_p is determined by limiting the larger velocity between (19) and (20) to $\dot{\phi}_{max}$.

$$k_p = \frac{r_w \min\{\dot{\phi}_{max}, \max\{\dot{\phi}_{iL}, \dot{\phi}_{iR}\}\} - \dot{\beta}_i}{\frac{r_i}{R_d} (\theta_d - \theta)} \quad (25)$$

where the max function is used to extract the maximum desired drive rate among all eight motors and the min function is used to compare it with the limit. After determining the gain value, the real driving command $\dot{\phi}_{iL}^{real}$ and $\dot{\phi}_{iR}^{real}$ can be obtained by substituting the k_p into (23) which will be fed into the platform.

IV. EXPERIMENTS AND RESULTS

In this section, the experimental setup with explanation is presented in detail, together with the results and discussions. The experiments were done using the hTetro platform as shown in Fig. 1. Fig. 6 shows the 2D map used for the experiment. The waypoints set for the robot are marked by red crosses. The same path is tested using all seven configurations and the results are discussed.

In order to test it in the real scenario, only waypoints containing the desired position and orientation are given to the robot. The waypoints are set to make the robot perform the zig-zag pattern and diagonal motion while keeping the orientation and steering angles with the controller proposed above. Sequences of the waypoints received by the robot are (0, 1.2), (0.5, 1.2), (0.8, 2.5), (0.3, 2.5), and (0, 5) with all dimensions measured in meters.

As shown in the Fig. 7, all seven configurations of the platform demonstrated the ability to follow the desired trajectory based on discrete waypoints and velocity commands under the Cartesian space. From the data collected, the minimum root mean square errors of the positions in X

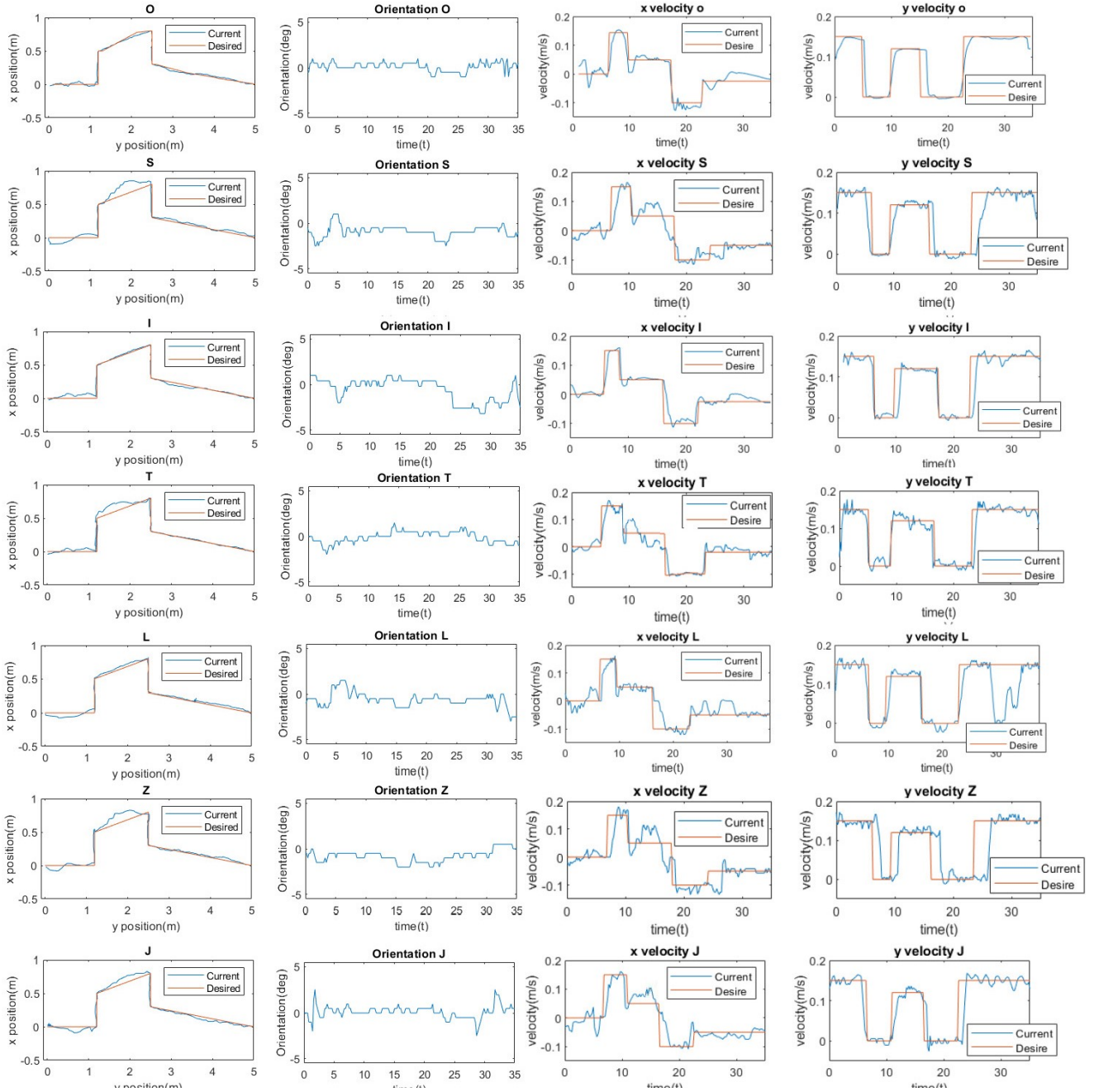


Fig. 7: Results of the proposed controller for each configuration of hTetro under Cartesian space.

and Y are implicitly 0.108m and 0.0623m which is from 'O' configuration, while the maximum root mean square errors are 0.129m and 0.16m which from 'S' configuration. The suspected reason for the weak performances in 'S', 'T', and 'Z' shapes is the non-linearity of the absolute encoder. Due to the phase difference of $\frac{\pi}{2}$ between two modules, the desired angles fall into the non-linear region of the absolute encoder and hence causing deviations. The ability to recover from disturbances is proved with the supplementary video.¹ In addition, when implementing the control strategy on the platform, some overshoot and oscillation response can be

observed in the velocity plot. The first reason we suspected is the joggle of the robot chassis which resulted in oscillation of the LIDAR. Secondly, imperfect tuning parameters of the motor controller might be another reason that would result in the oscillation in the velocity plot. These two issues are technical problems related to the fabrication of the platform.

V. CONCLUSIONS

In this paper, we presented the kinematic modeling and path tracking controller design of a novel modular reconfigurable cleaning robot with the usage of four differential drive modules. The usage of differential drive units to replace individual steering drive units helps to avoid the kinematic

¹ <https://1drv.ms/v/s!AuXDySZjV7Lddb44kt2bOHUA0Fg?e=1Efijq>

singularity. Kinematics modeling was done considering the self-reconfiguration of the hTetro robot into seven forms. The mapping of the ICR location enables the robot to decouple the linear and angular motion under Cartesian space. Additionally, the velocity controllers regulate the kinematic and hardware constraints of the platform making it able to fulfil the kinematic constraints under the transition period. Experiments on path tracking and overcoming disturbances were performed. The results reflect the ability of trajectory following and fast recovery from disturbances. Future research will focus on improvement on the robustness of platform, and dynamic controller design considering the influence of the cleaning brushes.

VI. ACKNOWLEDGMENT

Anonymous reviewers of the manuscript are greatly acknowledged for their valuable comments which improved the manuscript significantly. We are thankful to Dr. Abdullah Aamir Hayat at Singapore University of Technology and Design (SUTD), Singapore for proofreading the manuscript. This project is supported by Singapore National Robotics R&D Program Office under the Grant NO. RGAST1702 and SUTD-MIT International Design Center.

REFERENCES

- [1] Y. Fei and C. Wang, "Self-repairing algorithm of lattice-type self-reconfigurable modular robots," *Journal of Intelligent & Robotic Systems*, vol. 75, pp. 193–203, Aug 2014.
- [2] V. Singh, S. M. Skiles, J. E. Krager, K. L. Wood, D. Jensen, and R. Sierakowski, "Innovations in Design Through Transformation: A Fundamental Study of Transformation Principles," *Journal of Mechanical Design*, vol. 131, 07 2009.
- [3] P. Veerajagadheswar, M. R. Elara, T. Pathmakumar, and V. Ayyalusami, "A tiling-theoretic approach to efficient area coverage in a tetris-inspired floor cleaning robot," *IEEE Access*, vol. 6, pp. 35260–35271, 2018.
- [4] V. Prabhakaran, M. R. Elara, T. Pathmakumar, and S. Nansai, "htetro: A tetris inspired shape shifting floor cleaning robot," in *2017 IEEE International Conference on Robotics and Automation (ICRA)*, pp. 6105–6112, May 2017.
- [5] M. Lee and T. S. Li, "Kinematics, dynamics and control design of 4wis4wid mobile robots," *The Journal of Engineering*, vol. 2015, no. 1, pp. 6–16, 2015.
- [6] T. L. Lam, H. Qian, and Y. Xu, "Omnidirectional steering interface and control for a four-wheel independent steering vehicle," *IEEE/ASME Transactions on Mechatronics*, vol. 15, pp. 329–338, June 2010.
- [7] M. A. Vilaplana, O. Mason, D. Leith, and W. Leithead, "Control of yaw rate and sideslip in 4-wheel steering cars with actuator constraints," vol. 3355, pp. 201–222, 01 2003.
- [8] Z. Lu, M. Lin, S. Wang, Y. Zhang, and Y. Yu, "Research on a new-style under-actuated omnidirectional mobile robot based on special coupling drive system," *IEEE Access*, vol. 7, pp. 152138–152148, 2019.
- [9] C. P. Connette, C. Parlitz, M. Hagele, and A. Verl, "Singularity avoidance for over-actuated, pseudo-omnidirectional, wheeled mobile robots," in *2009 IEEE International Conference on Robotics and Automation*, pp. 4124–4130, May 2009.
- [10] C. Connette, M. Hgele, and A. Verl, "Singularity-free state-space representation for non-holonomic, omnidirectional undercarriages by means of coordinate switching," in *2012 IEEE/RSJ International Conference on Intelligent Robots and Systems*, pp. 4959–4965, Oct 2012.
- [11] A. Dietrich, T. Wimbck, A. Albu-Schffer, and G. Hirzinger, "Singularity avoidance for nonholonomic, omnidirectional wheeled mobile platforms with variable footprint," in *2011 IEEE International Conference on Robotics and Automation*, pp. 6136–6142, May 2011.
- [12] C. P. Connette, A. Pott, M. Hgele, and A. Verl, "Addressing input saturation and kinematic constraints of overactuated undercarriages by predictive potential fields," in *2010 IEEE/RSJ International Conference on Intelligent Robots and Systems*, pp. 4775–4781, Oct 2010.
- [13] M. Sorour, A. Cherubini, P. Fraisse, and R. Passama, "Motion discontinuity-robust controller for steerable mobile robots," *IEEE Robotics and Automation Letters*, vol. 2, pp. 452–459, April 2017.
- [14] M. Sorour, A. Cherubini, R. Passama, and P. Fraisse, "Kinematic modeling and singularity treatment of steerable wheeled mobile robots with joint acceleration limits," in *2016 IEEE International Conference on Robotics and Automation (ICRA)*, pp. 2110–2115, May 2016.
- [15] M. Sorour, A. Cherubini, A. Khelloufi, R. Passama, and P. Fraisse, "Complementary-route based icr control for steerable wheeled mobile robots," *Robotics and Autonomous Systems*, vol. 118, pp. 131 – 143, 2019.
- [16] R. Oftadeh, R. Ghabcheloo, and J. Mattila, "Time optimal path following with bounded velocities and accelerations for mobile robots with independently steerable wheels," in *2014 IEEE International Conference on Robotics and Automation (ICRA)*, pp. 2925–2931, May 2014.
- [17] V. Pitknen, A. Tikanmki, A. Kempainen, and J. Rning, "Path following controller for planar robots with articulated, actuated and independently steerable velocity-limited wheels," in *2017 IEEE International Conference on Robotics and Automation (ICRA)*, pp. 2433–2440, May 2017.
- [18] C. Stger, A. Mueller, and H. Gattringer, "Dynamic model-based control of redundantly actuated, non-holonomic, omnidirectional vehicles," pp. 69–78, 01 2016.
- [19] C. Stger, A. Mller, and H. Gattringer, "Kinematic analysis and singularity robust path control of a non-holonomic mobile platform with several steerable driving wheels," in *2015 IEEE/RSJ International Conference on Intelligent Robots and Systems (IROS)*, pp. 4140–4145, Sep. 2015.
- [20] T. T. Tun, L. Huang, R. E. Mohan, and S. G. H. Matthew, "Four-wheel steering and driving mechanism for a reconfigurable floor cleaning robot," *Automation in Construction*, vol. 106, p. 102796, 2019.